Chemical genetic approaches for target validation

Wel, T. van der

7

Summary & Future prospects

The aim of the research described in this thesis was to develop a chemical genetic strategy that can be used for target engagement and target validation studies.

Target engagement and target validation in drug discovery

Chapter 1 provided an overview of the current multi-stage drug discovery and development process. The initial stage of target validation remains a major challenge and relies on the availability of chemical tools to study the engagement of drugs to their intended target. Chemical probes with a covalent, irreversible mode of action can serve as powerful tools to visualize target engagement. However, these probes have to meet strict requirements in terms of potency, selectivity and cell permeability and the development of such probes can be a challenge on its own. The field of chemical genetics provides means to improve the potency and selectivity of small molecules by not only modifying the ligand, but also by engineering the protein target. Although different approaches have been reported, not all are applicable for target engagement studies. The engineered, mutant proteins often suffer from distorted protein folding, reduced catalytic activity or other functional defects. Moreover, current chemical genetic strategies all rely on the overexpression of a mutant protein, which may induce artefacts and disturbs cellular physiology. Novel strategies and probes are thus required to address these issues.

Chemical genetics to visualize engineered kinases and their target engagement

Chapter 2 introduced a chemical genetic strategy that allows visualization of engineered kinases and their target engagement. The non-receptor tyrosine kinase feline sarcoma oncogene (FES) was selected as exemplary target in this study. Currently, there are no suitable chemical tools available for target validation of FES. Furthermore, FES does not possess targetable cysteine residues in its catalytic pocket, rendering it difficult to develop chemical probes that can report on its target engagement.

In silico mutant design based on a previously reported crystal structure of FES revealed residues suitable for mutagenesis into a cysteine. Expression, purification and biochemical profiling of these mutants revealed that the DFG-1 residue Ser700 is an excellent position to mutate into a cysteine without affecting kinase activity, substrate recognition or SH2 domain binding profile. Subsequent design and synthesis of electrophilic derivatives of the reversible, broad-spectrum kinase inhibitor TAE684 resulted in the identification of WEL028 as a mutant-specific inhibitor of FES^{S700C} with low-nanomolar *in vitro* and *in situ* potencies (Figure 7.1A).

Kinome-wide selectivity screening revealed that WEL028 has a greatly improved selectivity profile compared to the starting point TAE684, with only a limited number of prominent off-targets.[1] Regardless, these few off-targets may limit applicability in functional studies, for example when these kinases are involved in the same signaling

pathway or associated with similar physiological processes as the kinase of interest. Further improvement of the selectivity of WEL028 may therefore be beneficial. Previous studies have shown that the *ortho*-methoxy substituent on the aniline moiety of TAE684 is positioned in a pocket formed by the kinase hinge region.[2] Incorporation of more bulky groups may therefore improve compound selectivity. FES, for example, has a relatively large pocket that can accommodate ethoxy- or isopropoxy-substituents, which could prove useful to eliminate some of the off-targets of WEL028 (Figure 7.1B).[3] In reverse,

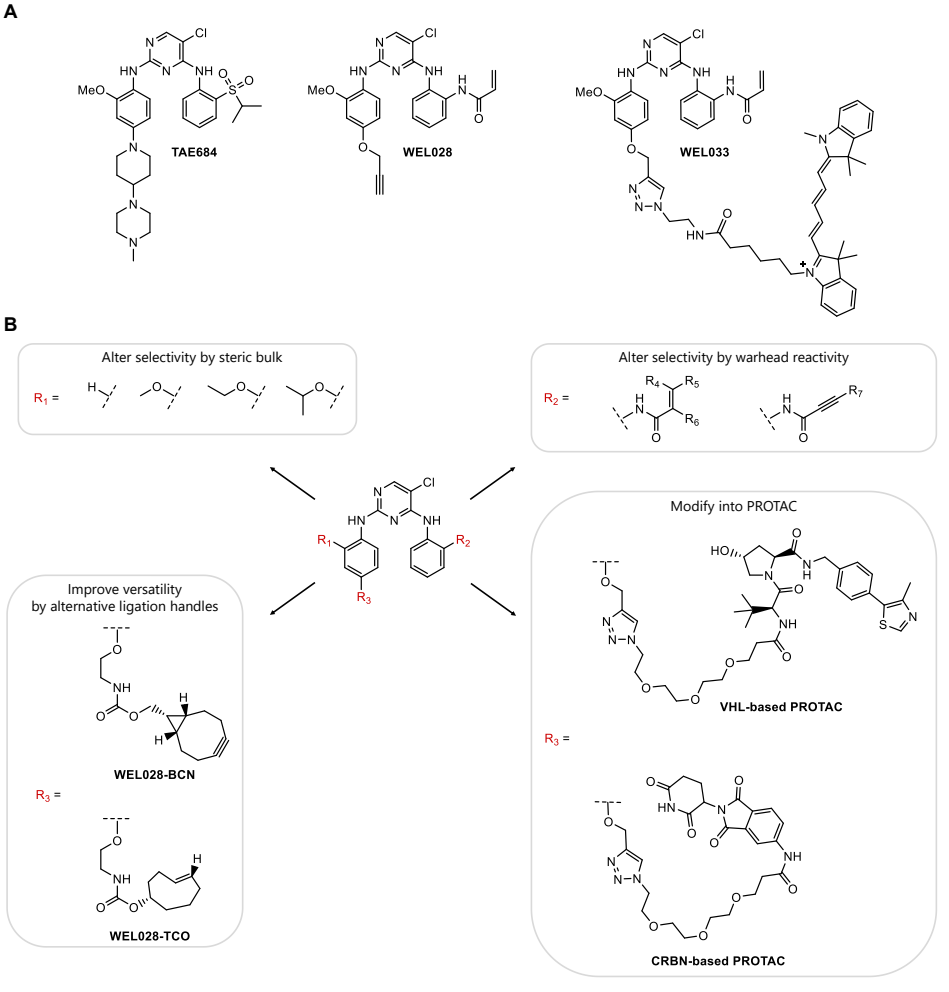

Figure 7.1 – Developed and proposed chemical genetic tools for kinase target validation. (A) Chemical structures of starting compound TAE684, mutant-specific FES^{S700C} inhibitor WEL028 and fluorescent probe WEL033. **(B)** Proposed WEL028 derivatives for improving selectivity, versatility in bioorthogonal conjugation or modification into PROTACs. BCN: bicyclononyne. TCO: trans-cyclooctene. VHL: Von Hippel-Lindau tumor suppressor. CRBN: protein cereblon.

removal of the *ortho*-methoxy moiety of WEL028 may allow for its use on a wider range of kinases that have larger amino acid residues in the hinge region. Undoubtedly, this structural change will also affect the compound's selectivity profile and kinome-wide selectivity screening should be performed on these WEL028 derivatives.

Another factor that affects covalent inhibitor selectivity is the reactivity of the nucleophilic (cysteine) residue and corresponding electrophile. Studies have shown that the pK_a of the cysteine sulfhydryl group is greatly affected by proximal amino acids[4,5], and that cysteines at the DFG-1 position are sufficiently reactive to undergo covalent addition to acrylamide warheads.[6–8] Since the nucleophilicity of the cysteine is inherent to its surrounding microenvironment and cannot readily be manipulated, tuning electrophile reactivity is increasingly considered as a means to improve covalent inhibitor selectivity.[9] Sufficiently reactive cysteines will also form covalent adducts with less reactive electrophiles, such as substituted acrylamides or butynamides (Figure 7.1B).[5] More detailed examination of the structure-reactivity relationship of WEL028 for engineered cysteine mutant kinases may therefore prove useful to further improve its kinome-wide selectivity, although the nucleophilicity of this engineered cysteine is likely to be different for each individual mutant kinase and should therefore be experimentally examined for each individual case.

Expanding the toolbox of complementary probes

Chapter 2 also provided evidence for a covalent, irreversible binding mode of WEL028, using a combination of LC-MS/MS and biochemical assays. Conjugation of a fluorescent Cy5 group to the alkyne moiety of WEL028 using click chemistry yielded the one-step probe WEL033 (Figure 7.1A), which enabled direct target engagement studies by fluorescently labeling recombinantly expressed FES^{S700C} but not FES^{WT} in cell lysate. One-step fluorescent probes such as WEL033 are useful tools to visualize target engagement *in vitro*, but usually have limited applicability for applications in living cells due to limited cell permeability. Two-step probes are therefore often better alternatives due to their lower molecular weight and improved cellular target engagement.[10] In chapter 2, WEL028 was used as a two-step probe to visualize target engagement on FES, but its alkyne handle requires copper-catalyzed click chemistry to conjugate reporter tags and the toxicity of the associated Cu^{I} species prohibits live cell imaging. In recent years, various alternative bioorthogonal groups have been reported that can allow conjugation without the use of copper, such as bicyclononyne (BCN) and trans-cyclooctene (TCO).[11] Incorporation of these handles onto the WEL028 scaffold (Figure 7.1B) would therefore allow for visualization of bound WEL028 targets in live cells, which may prove useful to investigate cellular localization of a kinase of interest during signaling processes.

Broader applicability of the developed chemical genetic toolbox was illustrated by gel-based labeling experiments on the DFG-1 cysteine mutant of four other kinases. It is unlikely, however, that a single chemical scaffold is able to target the entire kinome. Although TAE684 is a promiscuous kinase inhibitor that inhibits 98 out of 296 tested kinases with an IC_{50} <100 nM[12], it targets kinases mainly in the tyrosine kinase (TK) and calcium/calmodulin-dependent protein kinase (CAMK) families (Figure 7.2A). Therefore, different chemotypes may be required to enable a more complete coverage of the kinome.

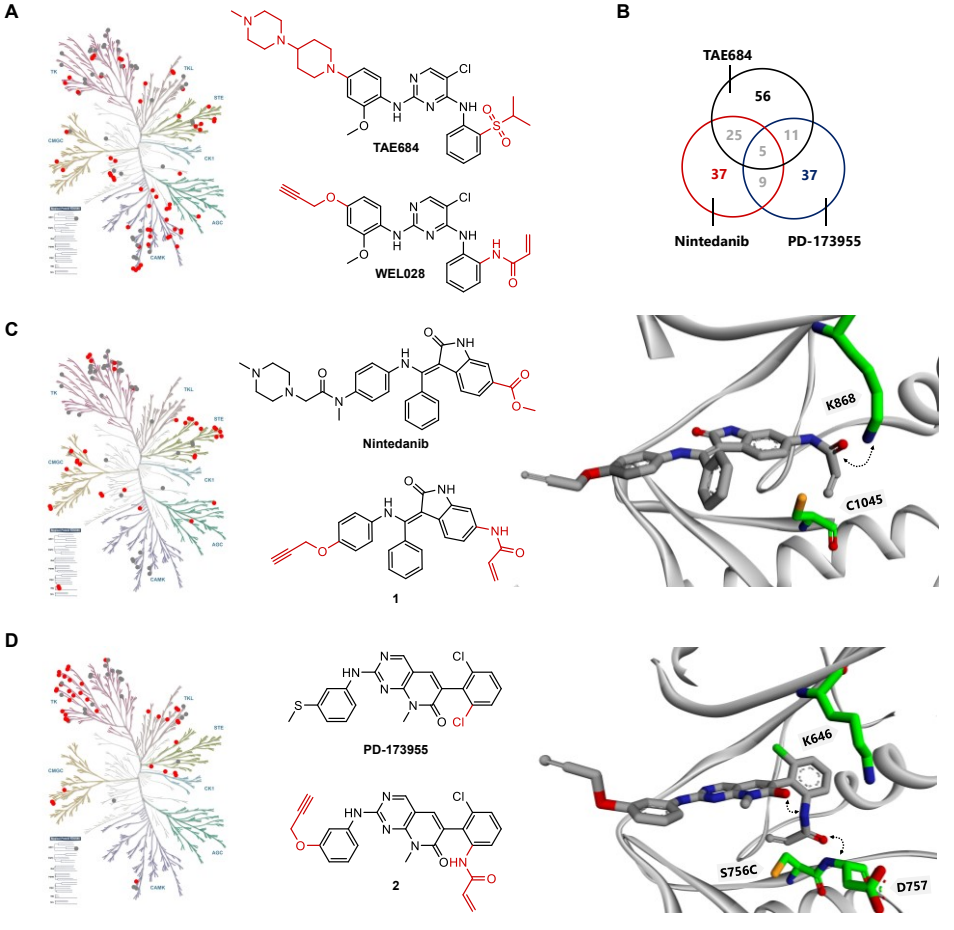

Figure 7.2 – Proposed chemotypes to expand the toolbox of complementary probes and improve kinome coverage. (A-D) Kinase target profile of the inhibitors TAE684, nintedanib and PD-173955 and proposed design of chemical probes **1** and **2** based on these inhibitors. Kinases with IC_{50} <100 nM as reported by Davis *et al.* were designated as targets.[1] Unique targets of TAE684 (A), nintedanib (C) and PD-173955 (D) are indicated as red dots, shared targets as grey dots. **(B)** Venn diagram visualizing unique and shared targets of the inhibitors. **(C, D)** Proposed binding mode of **1** and **2** in crystal structure (C: VEGFR2 kinase domain, PDB: 3c7q; D: EPHA2 kinase domain, PDB: 5ia3).[13,14] Structures were manually modified. Dotted arrows indicate potential interactions that may aid in positioning of the acrylamide warhead to undergo covalent addition to the DFG-1 cysteine. Kinome illustrations were rendered using KinMap (www.kinhub.org/kinmap), reproduced courtesy of Cell Signaling Technology, Inc. (www.cellsignal.com).

Davis *et al.* previously reported on the comprehensive target profile of 38 kinase inhibitors[1] and examination of these profiles revealed that the inhibitors nintedanib (VEGFR/FGFR/PDGFR inhibitor) and PD-173955 (BCR-ABL/SRC inhibitor) have a complementary profile to TAE684 with few overlapping targets (Figure 7.2B). For example, nintedanib has a good coverage of the STE subfamily (Figure 7.2C) and PD-173955 covers members of the tyrosine kinase-like (TKL) subfamily along with several non-receptor TKs (Figure 7.2D). Inspection of crystal structures of nintedanib (in VEGFR2 kinase domain, PDB: 3c7q) and PD-173955 (in EPHA2 kinase domain, PDB: 5ia3) revealed that minor structural modifications of these compounds may provide chemical probes with electrophilic warheads in close proximity of the respective DFG-1 residues (Figure 7.2C, D, compound **1** and **2**). Interestingly, interactions between the acrylamide carbonyl of **1** with a catalytic lysine may position its warhead in the appropriate conformation to undergo a Michael addition to the DFG-1 cysteine (Figure 7.2C), in a similar way as predicted in docking studies with WEL028 in the crystal structure of FES. Compound **2** probably does not reach far enough into this pocket to interact with Lys646, but hydrogen bonding between the acrylamide carbonyl and protein backbone amide might adequately position its warhead for covalent addition in a similar fashion (Figure 7.2D). Both chemical scaffolds could thus provide useful additions to the chemical genetic toolbox to improve kinome coverage.

Precise gene editing and complementary probes for target validation of FES kinase

Chapter 3 applied the combination of FES^{S700C} and its mutant-specific probes to study the role of FES activity during differentiation of myeloid cells. CRISPR/Cas9 gene editing was employed for mutagenesis of the genomic *FES* locus, which resulted in a homozygous HL-60 FES^{S700C} mutant cell line. Endogenous FES^{S700C} could be visualized in lysates of differentiated HL-60 cells using fluorescent probe WEL033. The ability to study target engagement by WEL028 in living HL-60 cells undergoing differentiation was instrumental to reveal that FES activity was not required for myeloid differentiation of HL-60 cells along the monocyte/macrophage lineage. This contradicted previous studies relying on transient overexpression or RNA knockdown of FES and demonstrates the benefit of acute, pharmacological modulation of endogenous kinase activity. Chapter 3 also illustrates the importance of being able to discern on-target from off-target effects. WEL028 disrupted differentiation of HL-60 cells at a higher concentration than required for complete FES inhibition. However, this effect also occurred in wild-type control cells and could thus be attributed to off-targets, which most likely are members of the MAP kinase family.

Chapter 3 concludes with a differentiation study in FES knockout cells, generated using CRISPR/Cas9. HL-60 FES^{KO} cells differentiated towards macrophages in a similar fashion as wild-type cells, suggesting that FES has no essential scaffold functions required for myeloid differentiation. It should be noted, however, that long-term ablation of FES expression may induce compensatory effects, *e.g.* by upregulation of other kinases. Kinase

inhibitors coupled to a ligand for VHL and CRBN ubiquitin ligases can function as proteolysis targeting chimeras (PROTACs), inducing acute proteolytic degradation of the targeted kinase by hijacking E3 ligases.[15–18] Active degradation of FES using a PROTAC might prove a valuable alternative for congenital knockout models. In addition to non-selective PROTACs that were previously reported to induce FES degradation[19], conjugation of WEL028 to a VHL or CRBN ligand (Figure 7.1B) could be considered as a more selective alternative.

It remains to be investigated whether FES is involved in the differentiation of other cell types, or downstream of other growth factor receptors. To this end, it would be interesting to use gene editing to mutate FES in inducible pluripotent stem cells (iPSCs) or hematopoietic stem cells (HSCs), since these can differentiate into a wide range of specialized cell types. A major advantage of using such a chemical genetic approach is the temporal control that allows acute modulation of FES activity at every stage of cell differentiation, opposed to permanent congenital knockout models where FES expression is absent already at the stem cell stage.

Chapter 4 showcased how the chemical genetic toolbox of chapter 2 and mutant cell line of chapter 3 can be used to study the role of kinases in cellular processes. Using a flow cytometry-based assay with GFP-expressing *E. coli*, it was shown that FES inhibition reduced the phagocytic uptake of HL-60 neutrophils. Examination of the FES substrate profile of chapter 2 led to the hypothesis that the tyrosine kinase SYK could be a potential FES substrate in this process. Transient co-expression experiments showed that FES phosphorylates SYK Y352 *in situ* and that FES interacts with SYK in a WEL028-dependent manner. Immunoblot analysis with phospho-specific antibodies revealed that blocking SYK Y352 phosphorylation abolished activation of the downstream proteins HS-1 and PLCγ2, two key players in phagocytosis.[20,21] These results suggest that FES mediates the activation of a signaling pathway involved in reorganization of the actin cytoskeleton required for bacterium internalization. Chapter 4 concludes with a model, proposing that FES may indirectly activate PLCγ2 to alter the membrane composition, resulting in its own dissociation from the membrane and thereby terminating the signaling input.

SYK is a central regulator of immune function and SYK inhibitors have therapeutic potential for cancer as well as autoimmune diseases, such as rheumatoid arthritis and lupus.[22,23] It would be interesting to explore, therefore, in what cell types and downstream of which receptors FES activates SYK, and whether FES inhibition may have similar therapeutic potential. In addition, great opportunities lay in the use of more advanced model systems, such as zebrafish. Zebrafish are increasingly appreciated as a valuable model to study host-pathogen interactions due to their genetic and physiological similarity to vertebrates and transparency that facilitates *in vivo* imaging.[24] Injection of vehicle- or WEL028-treated FES^{S700C} immune cells into the circulation of live fish suffering from

(bacterial) infection would be a suitable experimental setup to investigate the role of FES in migration of immune cells to the site of infection (Figure 7.3A). In combination with high-resolution (fluorescence) imaging techniques, this may provide valuable insights in FES immunobiology.

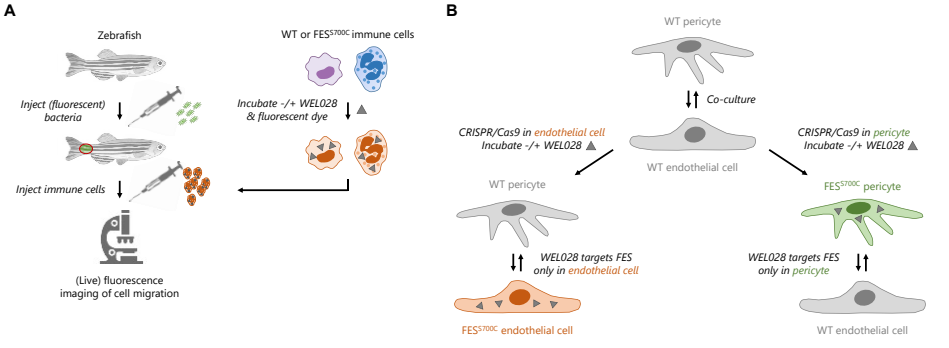

7.3 – Future applications of the chemical genetic toolbox to study FES biology. (A) Experimental setup that allows *in vivo* evaluation of acute FES inhibition by complementary probe WEL028. Zebrafish are injected with fluorescent bacteria to generate an infection. Next, wild-type or CRISPR/Cas9-modified FES^{S700C} immune cells are incubated with WEL028 and fluorescently labeled with a live-cell dye, followed by injection into the zebrafish. High-resolution fluorescence microscopy can be used to visualize immune cell migration *in vivo*, and study the effects of FES inhibition in this process. **(B)** Exemplary application to modulate FES activity with cellular specificity during blood vessel formation. The generation of new blood vessels is directed by complex cross-talk between endothelial cells and pericytes. CRISPR/Cas9 gene editing can be used to introduce the S700C mutation in the *FES* locus of one of these cell types, which enables cell type-specific inhibition of FES exclusively in either endothelial cells or pericytes.

Phagocytosis is not only important for elimination of pathogens, but also essential for the elimination of apoptotic cells and tissue homeostasis.[20] In the brain, for example, microglia survey the microenvironment and phagocytose dying neurons to prevent tissue damage.[25] However, microglia can also phagocytose protein aggregates that occur in neurodegenerative diseases (*e.g.* amyloid-β in Alzheimer's disease and α-synuclein in Parkinson's).[26–28] Very recently, studies have shown that a naturally occurring, rare genetic variant of PLCγ2 in microglia results in a P522R mutation that moderately increases its phospholipase activity.[29] This variant is protective against neurodegenerative diseases, such as Alzheimer's, Lewy body dementia and frontotemporal dementia, and increases the likelihood of longevity.[30,31] It would be interesting to investigate whether FES also indirectly activates PLCγ2 in microglia and whether FES activation has neuroprotective effects in models for these diseases.

Internalization of immunoreceptors is the fundamental process of phagocytosis. It remains to be seen whether FES plays a more general role in the internalization of other receptors. FES is not exclusively expressed in immune cells, but also in endothelial, epithelial and neuronal cell types.[32] Substrate and SH2 domain binding profiling revealed many cell surface receptors (*e.g.* VEGFR1/2, PDGFRB, CD79A, EPHA1/2) as potential FES substrates or binding partners. FES has been implicated in physiological processes

associated to some of these receptors, such as blood vessel formation and angiogenesis downstream of VEGFR in vascular endothelial cells.[33–35] The role of kinase activity in this process is particularly challenging to study, since the formation of blood vessels involves multiple cell types, including endothelial cells and pericytes.[36] Moreover, it remains a major challenge to achieve cellular specificity using pharmacological agents. The here presented chemical genetic approach would be ideally suited to investigate the cell type-specific function of FES in such complex biological processes, since it allows mutagenesis of FES in one specific cell type, whereas wild-type FES in other surrounding cell types is not affected (Figure 7.3B). Angiogenesis is essential for tumor growth, invasion and the development of metastasis, and a role for FES in this process would thus render it a potential therapeutic target for various types of cancer.[37]

Chemical genetics to achieve subtype-selective inhibition of DAGLs

Chapter 5 describes the first steps towards a chemical genetic strategy to achieve subtype-selective inhibition of the serine hydrolase DAGLα. Various positions in the DAGLα active site were mutated into a cysteine and the corresponding mutants were recombinantly expressed. Activity-based protein profiling with the two activity-based probes (ABPs) MB064 and DH379 and two substrate hydrolysis assays with PNPB and SAG were used for biochemical characterization of the DAGLα mutants. This revealed a general trend that mutation of residues in one pocket exhibited greatly reduced ABP labeling intensity and hydrolase activity, whereas mutations in another pocket were mostly tolerated. Design and synthesis of mutant-specific inhibitors based on a homology model[38] led to the identification of compound **4** (Figure 7.4F) as a an inhibitor of DAGLα^{L651C} but not DAGLα^{WT} or other DAGLα mutants. In addition, it showed selective inhibition of DAGLα over DAGLβ using competitive ABPP on mixed lysates of both DAGL subtypes. Compound **4**, however, showed a biphasic dose-response curve in all employed assays, suggesting two distinct binding events. The most potent interaction corresponded to a covalent, irreversible binding event of Cys651 to the bromoacetamide warhead of **4**, whereas the other interaction likely resembled a reversible binding event of catalytic Ser472 to the α-keto group. Further optimization of **4** is required prior to application of this chemical genetic strategy in cellular model systems.

The question arises whether the same chemical genetic approach could also be applied to generate subtype-selective inhibitors of DAGLβ. Mutagenesis of the homologous residue Met639 into a cysteine resulted in partially preserved labeling intensities by probes MB064 and DH379 (~50% compared to WT, Figure 7.4A-C), similar protein expression levels (Figure 7.4D) and slightly reduced hydrolase activity based on the PNPB substrate assay (~75% activity compared to WT, Figure 7.4E). Although compound **3** and **4** showed a 10-fold higher potency on DAGLβ^{M639C} compared to DAGLβ^{WT} (Figure 7.4G, H), this mutant-specific effect is more moderate than observed for DAGLα. It remains to

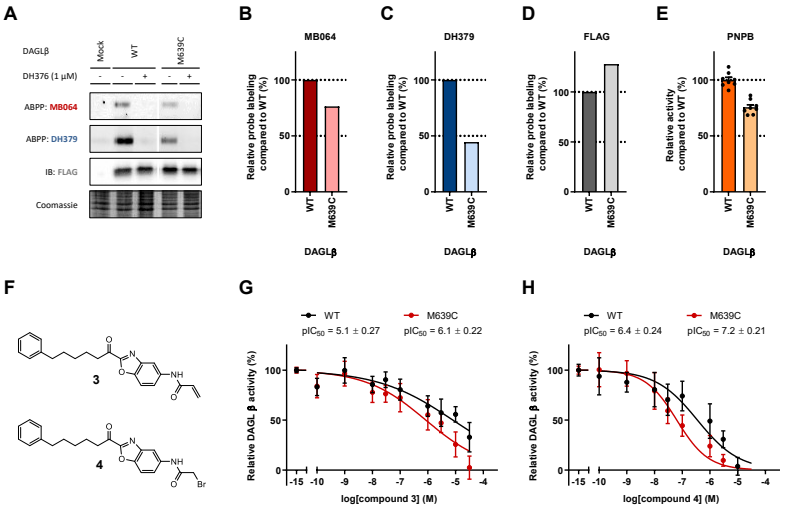

Figure 7.4 – DAGLβ mutant homolog M639C is expressed and active but less sensitive towards inhibition by complementary inhibitors than DAGLα^{L651C}. (A-D) Recombinantly expressed DAGLβ^{WT} and DAGLβ^{M639C} analyzed by activity-based protein profiling using probes MB064 (500 nM, 15 min, rt) and DH379 (1 μM, 15 min, rt). Protein expression was verified by anti-FLAG immunoblot. Band intensities were corrected for protein loading and normalized to wild-type control (N = 1). **(E)** Biochemical activity of DAGLβ^{WT} and DAGLβ^{M639C} analyzed by PNP-butyrate hydrolysis assay. Activity was determined using slope of reaction progress curve in linear range and normalized to wild-type control (N = 2, n = 4). **(F)** Chemical structures of compounds 3 and 4. **(G, H)** Dose-response curves of 3 (G) and 4 (H) on DAGLβ^{WT} and DAGLβ^{M639C}, determined using PNPB hydrolysis assay (N = 2, n = 4 for vehicle, N = 2, n = 2 for inhibitor-treated). Data represent means ± SEM.

be investigated, therefore, whether this potency increase results from irreversible, covalent addition of Cys639 to the electrophilic warheads of **3** and **4**.

A particularly interesting future application of a chemical genetic approach for DAGLα would involve the generation of genetically engineered mice that express the corresponding mutant exclusively in specific (brain) cell types. This allows one to modulate DAGLα activity in an acute and dynamic fashion with a cellular specificity that is very challenging to achieve by conventional medicinal chemistry efforts. Consequently, this will contribute to our understanding of DAGLα-dependent lipid signaling in different brain cell types and aid in the validation of DAGLα as a therapeutic target for various diseases related to the central nervous system, such as metabolic disorders and neurodegenerative diseases.[39]

Identification of reversible MAGL inhibitors: towards future drugs and chemical genetic tools

The serine hydrolase MAGL is responsible for degradation of the lipid 2-AG in the brain, which is synthesized by DAGLα.[40] To generate tools to modulate both the synthesis of 2-AG (by DAGLα, chapter 5) and its degradation, it was explored whether a chemical genetic

strategy could be applied to MAGL. In contrast to DAGLα, information about the MAGL protein structure is available. A structure of MAGL co-crystallized with Johnson & Johnson`s inhibitor ZYX304 (PDB: 3pe6)[41] was used to select active site residues for mutagenesis into a cysteine (Figure 7.5A). The corresponding mutants were recombinantly expressed and biochemically characterized. ABPP analysis with broad-spectrum probe FP-TAMRA and tailored MAGL probe LEI463 (Figure 7.5B) showed that some mutants were more effectively labeled by one of these ABPs than by the other (R^2 = 0.66, Figure 7.5C, D). This phenomenon was also observed for DAGLα mutants in chapter 5. Immunoblot analysis

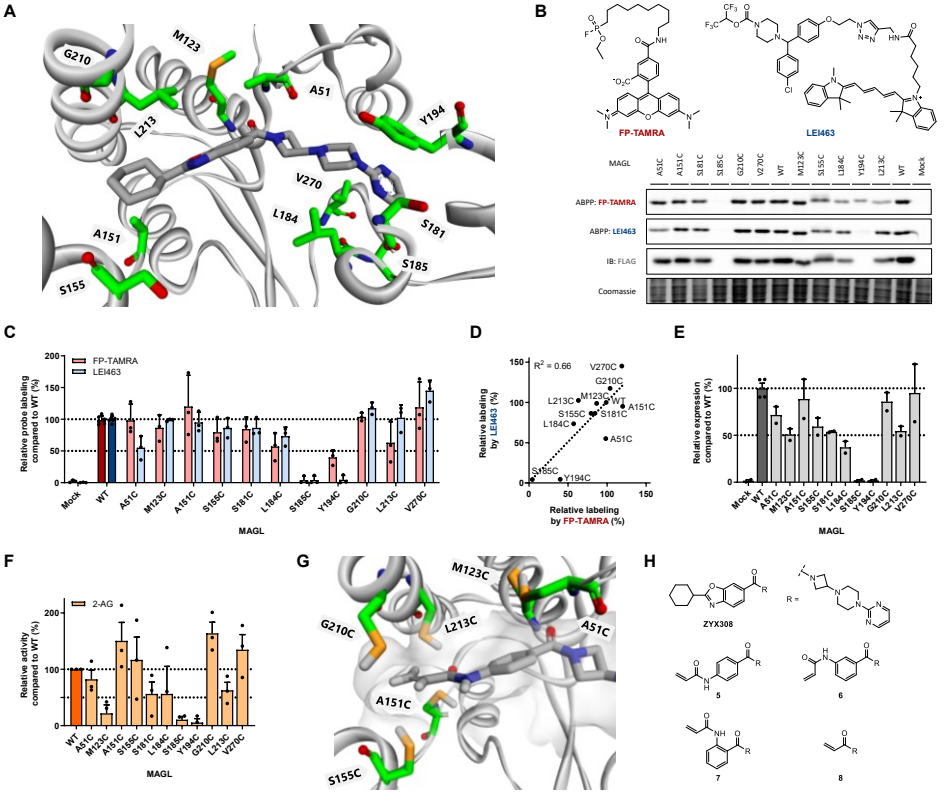

Figure 7.5 – Design of MAGL cysteine point mutants and characterization by activity-based protein profiling and substrate assays. (A) Location of mutated active site residues in MAGL crystal structure with inhibitor ZYX304 (PDB: 3pe6).[41] **(B, C)** Recombinantly expressed MAGL mutants analyzed by activity-based protein profiling using probes FP-TAMRA (500 nM, 20 min, rt) and LEI463 (100 nM, 20 min, rt). Protein expression levels were determined by anti-FLAG immunoblot. Band intensities were normalized to wild-type control (N = 3, individual transfections). **(D)** Correlation between FP-TAMRA and LEI463 labeling intensities. **(E)** Relative expression of MAGL mutants compared to wild-type. Band intensities were corrected for protein loading and normalized to wild-type control (N = 3, individual transfections). **(F)** Biochemical activity of DAGLα mutants analyzed by 2-AG hydrolysis assay. Activity was determined using slope of reaction progress curve in linear range and normalized to wild-type control (N = 3, individual transfections measured in n = 4 technical replicates). **(G)** Design of proposed irreversible inhibitor **5** to covalently target indicated cysteines in this pocket. **(H)** Structures of designed and synthesized ZYX304 analogs to covalently target MAGL cysteine mutants. Compounds **5**-**8** did not inhibit wild-type MAGL nor any of the tested mutants A151C, S155C and G210C (pIC_{50} <5 in 2-AG hydrolysis assay). Data represent means ± SEM.

revealed that mutants S185C and Y194C were not expressed (Figure 7.5E), suggesting that these mutations result in a unstable protein fold that is prone to degradation. Three mutants (M123C, S185C and Y194C) showed a major reduction (> 80%) in 2-AG hydrolysis activity, whereas the activity of S181C, L184C and L213C was reduced by approximately 50% (Figure 7.5F). In most cases, these reductions can be ascribed to lower expression levels. Other mutants showed 2-AG hydrolysis activity comparable to or even higher than wild-type (A51C, A151C, S155C, G210C and V270C). Interestingly, most of these active mutants were located in the cyclohexyl-benzoxazole binding pocket (Figure 7.5A and G). Acrylamide-derivatized ZYX304 analogs **5**-**8** were designed and synthesized to target (one of) these cysteine mutants (Figure 7.5H). Compounds were tested in dose-response experiments, which revealed that all derivatives had greatly diminished inhibitory potency on both wild-type MAGL and tested mutants A151C, S155C and G210C (pIC_{50} < 5 in 2-AG hydrolysis assay). This suggests that the cyclohexyl-benzoxazole group may be required for initial binding in the active site, or that the cysteine residues cannot be targeted by the acrylamide warhead of these compounds. Another possibility is that the acrylamide is not sufficiently reactive to undergo Michael addition to the cysteines under the employed assay conditions, as was also observed in chapter 5 for DAGLα. It may be useful to explore whether compounds bearing more reactive warheads do show a mutant-specific inhibition profile. Alternatively, other MAGL mutants could be selected for structure-based design of new derivatives, such as V270C, the MAGL homolog of DAGLα^{L651C}, directly adjacent to the catalytic His269 residue.

Chapter 6 reports on the optimization and miniaturization of a natural substrate-based activity assay for MAGL. This assay was then used for a high-throughput screening campaign on 233,820 compounds, which resulted in 1,142 confirmed actives. Deselection assays and hit triaging reduced this number to a list of 50 compounds that were profiled in dose-response experiments. Validation of these hits in an orthogonal competitive ABPP experiment led to a selection of 7 compounds that constitute starting points for the development of novel, reversible MAGL inhibitors. Blockage of 2-AG hydrolysis with MAGL inhibitors may prove beneficial for a wide variety of disorders, including Tourette syndrome, neuroinflammation, anxiety, pain and cancer.[42–47] In addition to their use as potential future therapeutics, these reversible hit compounds may be used for the design of chemical genetic tools as alternative for the ZYX304 scaffold.

Integration of chemical genetics in drug discovery

The development of new therapeutics depends on our understanding of the protein targets that are targeted by these drugs. The potential compensatory effects and lack of temporal control using genetic techniques as well as the lack of selective pharmacological modulators to acutely perturb protein function contribute to the fact that target validation remains a major challenge in current drug discovery.

As demonstrated in this thesis, the use of chemical genetic approaches may provide novel opportunities to aid in the validation of putative therapeutic targets. The specificity achieved by the use of an engineered, mutant protein allows one to apply the same chemical probe on a variety of different targets within a larger protein family, such as kinases or serine hydrolases. In addition, mutagenesis of amino acid residues into a reactive cysteine also allows one to target protein classes that completely lack nucleophilic residues in their binding site and are thus challenging to target with conventional chemical probes.

The generation of a homozygous mutant cell line as an endogenous model system is one of the key steps in the developed chemical genetic approach. Tremendous advances in gene and base editing technologies are expected to improve the efficiency and throughput of site-directed mutagenesis in cells. It would be interesting to explore whether fluorescent chemical probes that covalently bind to the engineered cysteine, such as WEL033, can be used to select and enrich for mutant cells in a fluorescence-activated cell sorting (FACS) setup. On the long term, it may be possible to generate site-directed mutagenesis libraries that can be universally applied to any (human) cell line of choice.[48,49] Broad applicability of the corresponding chemical probes is another prerequisite for effective integration in the drug discovery process, since it circumvents laborious optimization of the probes prior to application in target validation studies. It would be particularly powerful to couple target engagement and target validation studies to techniques that allow unbiased, global identification and quantification of target-specific downstream cellular processes, *e.g.* phosphoproteomics for kinases and lipidomics for lipases.

Concluding remarks

In this thesis, it was demonstrated that the field of chemical genetics can provide powerful tools to aid in target validation. Chemical genetics combines the specificity of genetic techniques with the acute and dynamic nature of pharmacology using small-molecule inhibitors. Compounds that bind in a covalent, irreversible fashion to mutant proteins harboring engineered cysteine residues are particularly useful by acting as chemical probes that can visualize target engagement. Chapter 2 showed the development of such a chemical genetic strategy that can be used for visualization of mutant kinases and their engagement by inhibitors. Potential applications in the target validation process were illustrated in chapter 3 and 4. The ability to perform comparative target engagement studies in wild-type and mutant cells was instrumental to refute the role of FES in myeloid differentiation of HL-60 cells. Chemical genetics can also be a valuable method to discover new enzyme substrates and functions, such as the identification of SYK as a substrate of FES and the discovery that FES plays a role in neutrophil phagocytosis. Chapter 5 demonstrated that a similar chemical genetic approach can be applied to other enzyme

classes, such as serine hydrolases. This also highlighted that successful design of mutant-specific inhibitors with a covalent binding mode greatly depends on structural information of the protein target, the reactivity of the introduced cysteine and the available (reversible) inhibitors. Chapter 6 reported on the use of high-throughput screening to identify novel chemical scaffolds with reversible binding modes that can be used for further optimization towards covalent probes or future therapeutics.

In conclusion, chemical genetics provides versatile pharmacological tools to modulate protein function with high specificity and can aid in the validation of proteins as therapeutic targets.

Acknowledgments

Bart Verschuren is kindly acknowledged for cloning and expression of DAGLβ variants, Rick Meijer for expression and characterization of MAGL mutants and Enrico Verpalen for synthesis of MAGL inhibitors.

Experimental procedures

General

All chemicals were purchased at Sigma Aldrich, unless stated otherwise. DNA oligos were purchased at Sigma Aldrich or Integrated DNA Technologies and sequences can be found in Supplementary Table 1. Cloning reagents were from Thermo Fisher. FP-TAMRA[50] and LEI463 were previously synthesized in-house and characterized by NMR and LC-MS. All cell culture disposables were from Sarstedt. Bacterial and mammalian protease inhibitor cocktails were obtained from Amresco. Assay enzymes (glycerol kinase from *Cellulomonas sp.*, product code G6142; glycerol-3-phosphate oxidase from *Streptococcus thermophilus*, product code G4388; horse radish peroxidase from *Horseradish*, product code 77332) were purchased from Sigma Aldrich. 2-Arachidonoylglycerol was purchased from Cayman Chemicals.

Cloning

Full-length wild-type mouse DAGLβ and human MAGL cDNA was obtained from Source Bioscience and cloned into pcDNA3.1 expression vectors as previously described.[38] Point mutations were introduced by site-directed mutagenesis and all plasmids were isolated from transformed XL10-Gold competent cells (prepared using *E. coli* transformation buffer set; Zymo Research) using plasmid isolation kits following the supplier's protocol (Qiagen). All sequences were verified by Sanger sequencing (Macrogen).

Supplementary Table 1 – List of oligonucleotide sequences.

ID	Name	Sequence
P1	MAGL_forw	CTTAAGCTTTGGTACCGCCGCCACCATGGAAACAGGACCTGAAG
P2	MAGL_rev	CATTCTAGATCACTCGAGACCGGTGGGTGGGGACGCAGTTC
P3	MAGL_A51C_forw	TTTGTGTCCCATGGATGTGGAGAGCACAGTGGC
P4	MAGL_A51C_rev	GCCACTGTGCTCTCCACATCCATGGGACACAAA
P5	MAGL_M123C_forw	CTTCTGGGCCACTCCTGTGGAGGCGCCATCGCC
P6	MAGL_M123C_rev	GGCGATGGCGCCTCCACAGGAGTGGCCCAGAAG
P7	MAGL_A151C_forw	ACTCATTTCGCCTCTAGTACTTTGCAATCCTGAATCTGC
P8	MAGL_A151C_rev	GCAGATTCAGGATTGCAAAGTACTAGAGGCGAAATGAGT
P9	MAGL_S155C_forw	GGTTCTTGCCAATCCGGAATGTGCAACAACTTTCAA
P10	MAGL_S155C_rev	TTGAAAGTTGTTGCACATTCCGGATTGGCAAGAACC
P11	MAGL_S181C_forw	TCGGGCCCATCGACTGCAGCGTGCTCTCTCG
P12	MAGL_S181C_rev	CGAGAGAGCACGCTGCAGTCGATGGGCCCGA
P13	MAGL_L184C_forw	CGGGCCCATCGACTCGAGCGTGTGCTCTCGGAATAAGAC
P14	MAGL_L184C_rev	GTCTTATTCCGAGAGCACACGCTCGAGTCGATGGGCCCG
P15	MAGL_S185C_forw	CGGGCCCATCGACTCGAGCGTGCTCTGTCGGAATAAGACAGA
P16	MAGL_S185C_rev	TCTGTCTTATTCCGACAGAGCACGCTCGAGTCGATGGGCCCG
P17	MAGL_Y194C_forw	TAAGACAGAGGTCGACATATGTAACTCAGACCCCCT
P18	MAGL_Y194C_rev	AGGGGGTCTGAGTTACATATGTCGACCTCTGTCTTA
P19	MAGL_G210C_forw	CTGAAGGTGTGCTTCTGCATCCAGCTGCTGAATGCCGTC
P20	MAGL_G210C_rev	GACGGCATTCAGCAGCTGGATGCAGAAGCACACCTTCAG
P21	MAGL_L213C_forw	GAAGGTGTGCTTCGGAATTCAATGCCTGAATGCCGTCTCA
P22	MAGL_L213C_rev	TGAGACGGCATTCAGGCATTGAATTCCGAAGCACACCTTC
P23	MAGL_V270C_forw	CAAGATTTATGAAGGCGCTTACCATTGCCTCCACAAGGAGCTT
P24	MAGL_V270C_rev	AAGCTCCTTGTGGAGGCAATGGTAAGCGCCTTCATAAATCTTG
P25	mDAGLb_forw	CTTAAGCTTTGGTACCGCCGCCACCATGCCGGGGATGGTGCTGTT
P26	mDAGLb_rev	GAGGCGGCCGCACCTGCCATACCGGTCGGTACACTTGAGCCGCCTT
P27	mDAGLb_M639C_forw	ATGCTGATTGACCACTGCCCTGACGTCATGATT
P28	mDAGLb_M639C_rev	AATCATGACGTCAGGGCAGTGGTCAATCAGCAT

Cell culture

HEK293T (human embryonic kidney) cells were obtained from ATCC and tested on regular basis for mycoplasma contamination. Cultures were discarded after 2-3 months of use. Cells were cultured at 37 °C under 7% CO2 in DMEM containing phenol red, stable glutamine, 10% (v/v) heat-inactivated newborn calf serum (Seradigm), penicillin and streptomycin (200 µg/mL each; Duchefa). Medium was refreshed every 2-3 days and cells were passaged two times a week at 80-90% confluence. One day prior to transfection, HEK293T cells were transferred from confluent 10 cm dishes to 15 cm dishes. Before transfection, medium was refreshed (13 mL). A 3:1 mixture of polyethyleneimine (PEI; 60 µg/dish) and plasmid DNA (20 µg/dish) was prepared in serum-free medium (2 mL) and incubated for 15 min at rt. The mixture was then dropwisely added to the cells, after which the cells were grown to confluence in 72 h. Cells were then harvested by suspension in PBS, followed by centrifugation (200 g, 5 min). Cell pellets were flash-frozen in liquid nitrogen and stored at -80 °C until membrane fraction preparation.

Membrane fraction preparation

Cell pellets were thawed on ice and homogenized by polytron (20,000 rpm, 3 x 7 s; SilentCrusher S, Heidolph) in lysis buffer A (20 mM HEPES pH 7.2, 2 mM DTT or 0.5 mM TCEP, 250 mM sucrose, 1 mM $MgCl_2$ and 25 U/mL benzonase). Suspensions were incubated on ice for 30 min to yield cell lysates. For preparation of membrane fractions, lysates were subjected to ultracentrifugation (93,000 *g,* 30

min, 4 °C; Beckman Coulter, Ti70 or Ti70.1 rotor) and pellets were homogenized in storage buffer B (20 mM HEPES pH 7.2, 2 mM DTT or 0.5 mM TCEP) by polytron (20,000 rpm, 1 x 10 s). Protein concentrations were determined using Quick Start™ Bradford Protein Assay (Bio-Rad). Membrane preparations were frozen in liquid nitrogen and stored at -80 °C until use.

Activity-based protein profiling (DAGLβ)

Membrane fractions (14 µL, 1.38 mg/mL) were incubated with inhibitor (0.5 µL in DMSO, 29x concentrated stock, 20 min, rt), followed by incubation with probe MB064 or DH379 (0.5 µL in DMSO, 30x concentrated stock, 15 min, rt). Reactions were quenched with 4x Laemmli buffer (5 µL, final concentrations 60 mM Tris pH 6.8, 2% (w/v) SDS, 10% (v/v) glycerol, 5% (v/v) β-mercaptoethanol, 0.01% (v/v) bromophenol blue) for 15 min at rt. Samples were resolved by SDS-PAGE on a 10% polyacrylamide gel (180 V, 75 min). Gels were scanned using Cy3 channel settings (605/50 filter; ChemiDoc™ MP System, Bio-Rad). Fluorescence intensity was corrected for protein loading determined by Coomassie Brilliant Blue R-250 staining and quantified with Image Lab (Bio-Rad).

Activity-based protein profiling (MAGL)

Cell lysate (14 µL, 1.38 mg/mL) was incubated with inhibitor (0.5 µL in DMSO, 29x concentrated stock, 20 min, rt), followed by incubation with probe FP-TAMRA or LEI463 (0.5 µL in DMSO, 30x concentrated stock, 20 min, rt). Reactions were quenched with 4x Laemmli buffer (5 µL, final concentrations 60 mM Tris pH 6.8, 2% (w/v) SDS, 10% (v/v) glycerol, 5% (v/v) β-mercaptoethanol, 0.01% (v/v) bromophenol blue) for 5 min at 95 °C. Samples were resolved by SDS-PAGE on a 10% polyacrylamide gel (180 V, 75 min). Gels were scanned using Cy3 and Cy5 multichannel settings (605/50 and 695/55 filters, respectively; ChemiDoc™ MP System, Bio-Rad). Fluorescence intensity was corrected for protein loading determined by Coomassie Brilliant Blue R-250 staining and quantified with Image Lab (Bio-Rad).

Immunoblot

Samples were resolved by SDS-PAGE and transferred to 0.2 µm polyvinylidene difluoride membranes by Trans-Blot Turbo™ Transfer system (Bio-Rad) directly after fluorescence scanning. Membranes were washed with TBS (50 mM Tris pH 7.5, 150 mM NaCl) and blocked with 5% milk in TBS-T (50 mM Tris pH 7.5, 150 mM NaCl, 0.05% Tween-20) for 1 h at rt. Membranes were then incubated with primary antibody in 5% milk in TBS-T (FLAG: 1:5000, 1 h at rt or o/n at 4 °C). Membranes were washed three times with TBS-T, incubated with matching secondary antibody in 5% milk in TBS-T (1:5000, 1 h at rt) and then washed three times with TBS-T and once with TBS. Imaging solution (10 mL luminol in 100 mM Tris pH 8.8, 100 µL ECL enhancer, 3 µL H_2O_2) was added and chemiluminescence was detected on ChemiDoc™ MP System. Primary antibody: monoclonal mouse anti-FLAG M2 (1:5000, Sigma Aldrich, F3156), secondary antibody: goat anti-mouse-HRP (1:5000, Santa Cruz, sc-2005).

PNP-butyrate hydrolysis assay (DAGLβ)

Assays were performed in 50 mM HEPES pH 7.0, 10 mM $CaCl_2$ in clear, flat-bottom 96-well plates (Greiner). Inhibitors were added from 40x concentrated stock solution in DMSO. DAGLβ-overexpressing membrane preparations (20 µg per well) were incubated with inhibitor for 20 min at rt in a total volume of 190 µL. Next, 10 µL substrate solution (PNP-butyrate in 1:1 mixture of DMSO/H_2O, final concentration 600 µM) was added. Absorbance at 420 nm was measured at 37 °C in 1 min intervals for 20 min on a GENios plate reader (Tecan). Final assay concentrations: 100 ng/µL DAGLβ-overexpressing membranes, 600 µM PNP-butyrate, 5% DMSO in a total volume of 200 µL. All measurements were performed in N = 2 (individual plates), n = 2 (technical replicates on same plate) or N = 2, n = 4 for controls, with $Z' \geq 0.6$.

2-AG hydrolysis assay (MAGL)

Assays were performed in HEMNB buffer (50 mM HEPES pH 7.4, 1 mM EDTA, 5 mM $MgCl_2$, 100 mM NaCl, 0.5% (w/w) BSA) in black, flat-bottom 96-well plates (Greiner). Inhibitors were added from 40x

concentrated stock solution in DMSO. MAGL-overexpressing membrane preparations (0.3 µg per well) were incubated with inhibitor for 20 min at rt in a total volume of 100 µL. Next, 100 µL assay mix containing glycerol kinase (GK), glycerol-3-phosphate oxidase (GPO), horse radish peroxidase (HRP), adenosine triphosphate (ATP), Amplifu™Red and 2-arachidonoylglycerol (2-AG) was added. Fluorescence (λ_{ex} = 535 nm, λ_{em} = 595 nm) was measured at rt in 5 min intervals for 60 min on a GENios plate reader (Tecan). Final assay concentrations: 1.5 ng/µL MAGL-overexpressing membranes, 0.2 U/mL GK, GPO and HRP, 125 µM ATP, 10 µM Amplifu™Red, 25 µM 2-AG, 5% DMSO, 0.5% ACN in a total volume of 200 µL. All measurements were performed in N = 2 (individual plates), n = 2 (technical replicates on same plate) or N = 2, n = 4 for controls, with Z' ≥ 0.6.

Data analysis, statistics and software

All shown data represent means ± SEM, unless indicated otherwise. Replicates are indicated in figure legends with N for biological and n for technical replicates, respectively. All modeling figures were rendered using Discovery Studio 2016 (BIOVIA).

For substrate hydrolysis assays, absorbance or fluorescence values were corrected for the average of the negative control (mock-membranes + vehicle). DAGLβ- or MAGL-overexpressing (wild-type or mutant) membranes incubated with vehicle served as a positive control. Slopes of the corrected data were determined in the linear interval. The Z'-factor for each assay plate was calculated using the formula $Z' = 1 - 3(\sigma_{pc} + \sigma_{nc})/(\mu_{pc} - \mu_{nc})$ with σ = standard deviation, µ = mean, pc = positive control and nc = negative control. Plates with Z' ≥ 0.6 were accepted for further analysis. For IC_{50} determination, slopes were normalized to the positive control and analyzed using 'Non-linear dose-response analysis with variable slope'. For curves with clear two-phase binding behavior, data were analyzed using 'Two sites – Fit logIC50' (GraphPad Prism 7.0).

References

1. Davis, M. I. *et al.* Comprehensive analysis of kinase inhibitor selectivity. *Nat. Biotechnol.* **29**, 1046–1051 (2011).
2. Hellwig, S. *et al.* Small-molecule inhibitors of the c-Fes protein-tyrosine kinase. *Chem. Biol.* **19**, 529–540 (2012).
3. Marsilje, T. H. *et al.* Synthesis, Structure-Activity Relationships, and in Vivo Efficacy of the Novel Potent and Selective Anaplastic Lymphoma Kinase (ALK) Inhibitor 5-Chloro-N2-(2-isopropoxy-5-methyl-4-(piperidin-4-yl)phenyl)-N4-(2-(isopropylsulfonyl)phenyl)pyrimidine-2,4-diam. *J. Med. Chem.* **56**, 5675–5690 (2013).
4. Garske, A. L., Peters, U., Cortesi, A. T., Perez, J. L. & Shokat, K. M. Chemical genetic strategy for targeting protein kinases based on covalent complementarity. *Proc. Natl. Acad. Sci. U. S. A.* **108**, 15046–15052 (2011).
5. Demont, D. *et al.* Acalabrutinib (ACP-196): A Covalent Bruton Tyrosine Kinase Inhibitor with a Differentiated Selectivity and In Vivo Potency Profile. *J. Pharmacol. Exp. Ther.* **363**, 240–252 (2017).
6. Lebraud, H. *et al.* In-gel activity-based protein profiling of a clickable covalent ERK1/2 inhibitor. *Mol. BioSyst.* **12**, 2867–2874 (2016).
7. Cohen, M. S., Hadjivassiliou, H. & Taunton, J. A clickable inhibitor reveals context-dependent autoactivation of p90 RSK. *Nat. Chem. Biol.* **3**, 156–160 (2007).
8. Tan, L. *et al.* Structure-guided development of covalent TAK1 inhibitors. *Bioorganic Med. Chem.* **25**, 838–846 (2017).
9. Flanagan, M. E. *et al.* Chemical and computational methods for the characterization of covalent reactive groups for the prospective design of irreversible inhibitors. *J. Med. Chem.* **57**, 10072–10079 (2014).
10. Sipthorp, J. *et al.* Visualization of Endogenous ERK1/2 in Cells with a Bioorthogonal Covalent Probe. *Bioconjug. Chem.* **28**, 1677–1683 (2017).
11. Devaraj, N. K. The Future of Bioorthogonal Chemistry. *ACS Cent. Sci.* **4**, 952–959 (2018).
12. Karaman, M. W. *et al.* A quantitative analysis of kinase inhibitor selectivity. *Nat. Biotechnol.* **26**, 127–132 (2008).
13. Hilberg, F. *et al.* BIBF 1120: Triple angiokinase inhibitor with sustained receptor blockade and good antitumor efficacy. *Cancer Res.* **68**, 4774–4782 (2008).
14. Heinzlmeir, S. *et al.* Chemical Proteomics and Structural Biology Define EPHA2 Inhibition by Clinical Kinase Drugs. *ACS Chem. Biol.* **11**, 3400–3411 (2016).
15. Crews, C. M. *et al.* Protacs: Chimeric molecules that target proteins to the Skp1-Cullin-F box complex for ubiquitination and degradation. *Proc. Natl. Acad. Sci.* **98**, 8554–8559 (2002).
16. Lai, A. C. & Crews, C. M. Induced protein degradation: An emerging drug discovery paradigm. *Nature Reviews Drug Discovery* **16**, 101–114 (2017).
17. Ottis, P. & Crews, C. M. Proteolysis-Targeting Chimeras: Induced Protein Degradation as a Therapeutic Strategy. *ACS Chemical Biology* **12**, 892–898 (2017).
18. Collins, I., Wang, H., Caldwell, J. J. & Chopra, R. Chemical approaches to targeted protein degradation through modulation of the ubiquitin–proteasome pathway. *Biochem. J.* **474**, 1127–1147 (2017).
19. Huang, H. T. *et al.* A Chemoproteomic Approach to Query the Degradable Kinome Using a Multi-kinase Degrader. *Cell Chem. Biol.* **25**, 88-99.e6 (2018).
20. Rosales, C. & Uribe-Querol, E. Phagocytosis: A Fundamental Process in Immunity. *BioMed Research International* **2017**, 1–18 (2017).
21. Castro-Ochoa, K. F., Guerrero-Fonseca, I. M. & Schnoor, M. Hematopoietic cell-specific lyn substrate (HCLS1 or HS1): A versatile actin-binding protein in leukocytes. *Journal of Leukocyte Biology* **105**, 881–890 (2019).
22. Ruzza, P., Biondi, B. & Calderan, A. Therapeutic prospect of Syk inhibitors. *Expert Opin. Ther. Pat.* **19**, 1361–1376 (2009).
23. Liu, D. & Mamorska-Dyga, A. Syk inhibitors in clinical development for hematological malignancies. *Journal of Hematology and Oncology* **10**, 145 (2017).
24. Torraca, V. & Mostowy, S. Zebrafish Infection: From Pathogenesis to Cell Biology. *Trends in Cell Biology* **28**, 143–156 (2018).
25. Aguzzi, A., Barres, B. A. & Bennett, M. L. Microglia: Scapegoat, Saboteur, or Something Else? *Science (80-.).* **339**, 156–161 (2013).
26. Glass, C. K., Saijo, K., Winner, B., Marchetto, M. C. & Gage, F. H. Mechanisms Underlying Inflammation in Neurodegeneration. *Cell* **140**, 918–934 (2010).
27. Sokolowski, J. D. & Mandell, J. W. Phagocytic clearance in neurodegeneration. *American Journal of Pathology* **178**, 1416–1428 (2011).
28. Brown, G. C. & Neher, J. J. Microglial phagocytosis of live neurons. *Nat. Rev. Neurosci.* **15**, 209–216 (2014).
29. Magno, L. *et al.* Alzheimer's disease phospholipase C-gamma-2 (PLCG2) protective variant is a functional hypermorph. *Alzheimer's Res. Ther.* **11**, 16 (2019).
30. Conway, O. J. *et al.* ABI3 and PLCG2 missense variants as risk factors for neurodegenerative diseases in Caucasians and African Americans 11 Medical and Health Sciences 1109 Neurosciences 06 Biological Sciences 0604 Genetics. *Mol. Neurodegener.* **13**, 53 (2018).

31. van der Lee, S. J. *et al.* A nonsynonymous mutation in PLCG2 reduces the risk of Alzheimer's disease, dementia with Lewy bodies and frontotemporal dementia, and increases the likelihood of longevity. *Acta Neuropathol.* **138**, 237–250 (2019).
32. Haigh, J., McVeigh, J. & Greer, P. The fps/fes tyrosine kinase is expressed in myeloid, vascular endothelial, epithelial, and neuronal cells and is localized in the trans-golgi network. *Cell growth Differ.* **7**, 931–44 (1996).
33. Sangrar, W., Mewburn, J. D., Vincent, S. G., Fisher, J. T. & Greer, P. A. Vascular defects in gain-of-function fps/fes transgenic mice correlate with PDGF- and VEGF-induced activation of mutant Fps/Fes kinase in endothelial cells. *J. Thromb. Haemost.* **2**, 820–832 (2004).
34. Kanda, S., Mochizuki, Y., Miyata, Y. & Kanetake, H. The role of c-Fes in vascular endothelial growth factor-A-mediated signaling by endothelial cells. *Biochem. Biophys. Res. Commun.* **306**, 1056–1063 (2003).
35. Kanda, S., Kanetake, H. & Miyata, Y. Downregulation of Fes inhibits VEGF-A-induced chemotaxis and capillary-like morphogenesis by cultured endothelial cells. *J. Cell. Mol. Med.* **11**, 495–501 (2007).
36. Sweeney, M. & Foldes, G. It Takes Two: Endothelial-Perivascular Cell Cross-Talk in Vascular Development and Disease. *Front. Cardiovasc. Med.* **5**, 154 (2018).
37. Bergers, G. & Benjamin, L. E. Tumorigenesis and the angiogenic switch. *Nature Reviews Cancer* **3**, 401–410 (2003).
38. Baggelaar, M. P. *et al.* Development of an activity-based probe and in silico design reveal highly selective inhibitors for diacylglycerol lipase-α in brain. *Angew. Chemie - Int. Ed.* **52**, 12081–12085 (2013).
39. Janssen, F. J. & van der Stelt, M. Inhibitors of diacylglycerol lipases in neurodegenerative and metabolic disorders. *Bioorganic Med. Chem. Lett.* **26**, 3831–3837 (2016).
40. Bisogno, T. *et al.* Cloning of the first sn1-DAG lipases points to the spatial and temporal regulation of endocannabinoid signaling in the brain. *J. Cell Biol.* **163**, 463–468 (2003).
41. Schalk-Hihi, C. *et al.* Crystal structure of a soluble form of human monoglyceride lipase in complex with an inhibitor at 1.35 A ° resolution. *Protein Sci.* **20**, 670–683 (2011).
42. Pasquarelli, N. *et al.* Evaluation of monoacylglycerol lipase as a therapeutic target in a transgenic mouse model of ALS. *Neuropharmacology* **124**, 157–169 (2017).
43. Hernández-Torres, G. *et al.* A reversible and selective inhibitor of monoacylglycerol lipase ameliorates multiple sclerosis. *Angew. Chemie - Int. Ed.* **53**, 13765–13770 (2014).
44. Chen, R. *et al.* Monoacylglycerol Lipase Is a Therapeutic Target for Alzheimer's Disease. *Cell Rep.* **2**, 1329–1339 (2012).
45. Kinsey, S. G., O'Neal, S. T., Long, J. Z., Cravatt, B. F. & Lichtman, A. H. Inhibition of endocannabinoid catabolic enzymes elicits anxiolytic-like effects in the marble burying assay. *Pharmacol. Biochem. Behav.* **98**, 21–27 (2011).
46. Griebel, G. *et al.* Selective blockade of the hydrolysis of the endocannabinoid 2-arachidonoylglycerol impairs learning and memory performance while producing antinociceptive activity in rodents. *Sci. Rep.* **5**, 7642 (2015).
47. Nomura, D. K. *et al.* Monoacylglycerol Lipase Regulates a Fatty Acid Network that Promotes Cancer Pathogenesis. *Cell* **140**, 49–61 (2010).
48. Zhou, Y. *et al.* High-throughput screening of a CRISPR/Cas9 library for functional genomics in human cells. *Nature* **509**, 487–491 (2014).
49. Mason, D. M. *et al.* High-throughput antibody engineering in mammalian cells by CRISPR/Cas9-mediated homology-directed mutagenesis. *Nucleic Acids Res.* **46**, 7436–7449 (2018).
50. Janssen, A. P. A. *et al.* Development of a Multiplexed Activity-Based Protein Profiling Assay to Evaluate Activity of Endocannabinoid Hydrolase Inhibitors. *ACS Chemical Biology* (2018). doi:10.1021/acschembio.8b00534